Available online at www.sciencedirect.com
ScienceDirect
Journal of Sound and Vibration 311 (2008) 973–990
JOURNAL OF SOUND AND VIBRATION
www.elsevier.com/locate/jsvi

Transmission of longitudinal wave at a plane interface between micropolar elastic and chiral solid half-spaces: Incidence from micropolar half-space

Aarti Khurana[1], S.K. Tomar*

Department of Mathematics, Panjab University, Chandigarh 160 014, India

Received 8 December 2006; received in revised form 29 July 2007; accepted 25 September 2007
Available online 5 November 2007

Abstract

Reflection and transmission phenomena of a plane longitudinal displacement wave impinging obliquely at a plane interface between a micropolar elastic solid half-space and a chiral elastic solid half-space are investigated. The incident wave is assumed to be striking at the plane interface after propagating through the micropolar elastic solid half-space. The reflection and transmission coefficients are obtained by utilizing two possible sets of boundary conditions, for a specific model and there values corresponding to two boundary conditions are also compared graphically. The effect of chirality parameter on various reflection and transmission coefficients have been noticed and shown graphically. Results of Lakhtakia et al. [Reflection of elastic plane waves at a planar achiral–chiral interface, *Journal of the Acoustical Society of America* 87 (1990) 2314–2318] and Miklowitz [The Theory of Elastic Waves and Waveguides, North-Holland, New York, 1978] have also been reduced as special cases from the present formulation.

1. Introduction

In a generalized granular solid continuum, the usual displacement field has to be supplemented by a microrotation field. Such a material is called a micropolar solid or a Cosserat solid, and may possess a negative Poisson's ratio [1,2]. An isotropic micropolar solid may be hemitropic [3], i.e., it is isotropic with respect to all proper orthogonal transformations but not with respect to reflections. Such a material is called mirror asymmetric or Chiral. Chiral materials, due to lack of geometric symmetry between an object and its mirror image, have been known in optics as *optically active materials*. This phenomenon of optical activity in substances has been known for nearly two centuries and was discovered independently by Arago [4] and Biot [5,6]. It has been extensively utilized by the physical chemists for characterizing the molecular structure. The physical phenomenon of chiral materials was first observed in optical spectrum due to the transverse nature of optical wave [7]. Bose [8] was the first person to develop artificial chiral composite materials. Artificial chiral

*Corresponding author.
E-mail addresses: aarti_maths@yahoo.com (A. Khurana), sktomar@yahoo.com (S.K. Tomar).
[1]Present address: D.A.V. College, Sector-10, Chandigarh 160 011, India.

0022-460X/$ - see front matter © 2007 Elsevier Ltd. All rights reserved.
doi:10.1016/j.jsv.2007.09.032

composites have been proposed and tailored at microwave frequencies for designing broadband absorbers and filters [8–10]. This gives rise to the idea that the chiral materials may also be applied in the elastic spectrum for designing broadband absorbers and impedance transformers. To attain this goal, the constitutive equations [11], and the governing equations [12] for non-centrosymmetric, isotropic micropolar materials have been proposed to describe the propagation characteristics of elastic waves in chiral media.

The linear theory for non-centrosymmetric, isotropic (hemitropic) micropolar elastic solids or mechanical active solids was developed by Kuvshinskii and Aero [13,14], Aero and Kuvshinskii [15], Eringen [16], Lakes and Benedict [11] and Nowacki [12]. They reported that the continuum is composed of randomly arranged springs, and hence, the microstructure possesses a screw-like property or a handedness. Such a medium undergoing a homogeneous deformation can support couple stresses and spin inertia. It is known that an effective chiral medium can be constructed by the helical arrangement of microstructures, e.g., the structural chiral inclusions or springs embedded in a host medium [3,17] and therefore, 6 independent wavenumbers are possible. Two of the wavenumbers represent non-dispersive longitudinal fields, while the remaining 4 are dispersive circularly polarized transverse fields [18]. The dispersion equations of the transverse fields also indicate that 2 transition frequencies of the dispersion equation divide the frequency response of the transverse wavenumbers into 3 varying groups and hence, the 4 transverse modes can only be distinguished in a specified frequency range [19].

Various researchers [20–22] have discussed the problems of reflection and transmission of plane waves at an interface between two semi-infinite media in perfect contact. Parfitt and Eringen [23] have discussed the reflection of plane waves from a flat boundary of micropolar elastic solid half-space. Tomar and Gogna [20,21] extended the investigations to a longitudinal microrotational wave and a longitudinal displacement wave impinging at a plane discontinuity between two micropolar elastic solid half-spaces in welded contact. Lakhtakia et al. [24] and Elphinstone and Lakhtakia [22] have presented the reflection/transmission phenomena for an incident plane wave propagating towards the achiral–chiral interface. Elphinstone and Lakhtakia [22] have mentioned that when a linearly polarized plane wave in an isotropic non-chiral medium encounters an interface with a chiral medium, the refracted plane waves are either longitudinal or transverse circularly polarized.

In the present paper, we have discussed the reflection/transmission phenomena of a plane longitudinal wave at a plane interface between a micropolar elastic solid half-space and an elastic chiral solid half-space. The incident wave is assumed to impinge obliquely through the micropolar elastic solid half-space. The variations of square of phase speeds of transverse circularly polarized plane waves of chiral medium with the frequency ratio are shown graphically. The reflection and transmission coefficients are computed using two possible sets of boundary conditions, for a specific model. The variations of modulus of various reflection and transmission coefficients with the angle of incidence are presented graphically. We have also shown graphically the effect of chirality parameter (C_3) on various reflection and transmission coefficients. The results of some earlier researchers are analogous with the limiting cases of the present formulation.

2. Formulation of the problem

Let x, y, z be the Cartesian coordinates. We consider a model consisting of a micropolar elastic solid half-space and an elastic chiral solid half-space, where both the half-spaces are separated by the plane interface $z = 0$. The force stress tensor τ_{ij} and the couple stress tensor m_{ij} for a micropolar elastic solid are given by (Ref. [25])

$$\tau_{ij} = \lambda u_{k,k}\delta_{ij} + \mu(u_{i,j} + u_{j,i}) + K(u_{j,i} - e_{ijk}\Phi_k), \tag{1}$$

$$m_{ij} = \alpha\Phi_{k,k}\delta_{ij} + \beta\Phi_{i,j} + \gamma\Phi_{j,i}, \tag{2}$$

where $\lambda, \mu, \alpha, \beta, \gamma$ and K are the material moduli, e_{ijk} is the permutation symbol, δ_{ij} is the Kronecker delta; u_i and Φ_i are the displacement and the microrotation vectors, respectively. Here, we have employed the usual summation convention on the repeated indices.

Following Eringen [25], the equations of motion in a micropolar elastic solid in the absence of body force and body couple densities are given by

$$(\lambda+2\mu+K)\nabla\nabla\cdot\mathbf{u}-(\mu+K)\nabla\times\nabla\times\mathbf{u}+K\nabla\times\mathbf{\Phi}=\rho\ddot{\mathbf{u}}, \tag{3}$$

$$(\alpha+\beta+\gamma)\nabla\nabla\cdot\mathbf{\Phi}-\gamma\nabla\times\nabla\times\mathbf{\Phi}+K\nabla\times\mathbf{u}-2K\mathbf{\Phi}=\rho J\ddot{\mathbf{\Phi}}, \tag{4}$$

where ρ is the density of the medium and J is the micro-inertia.

Introducing the scalar potentials q and ξ; the vector potentials $\mathbf{U}$ and $\mathbf{\Pi}$, as follows:

$$\mathbf{u}\equiv\nabla q+\nabla\times\mathbf{U};\quad \mathbf{\Phi}\equiv\nabla\xi+\nabla\times\mathbf{\Pi};\quad \nabla\cdot\mathbf{\Pi}=\nabla\cdot\mathbf{U}=0. \tag{5}$$

By using (5) into Eqs. (3)–(4), Parfitt and Eringen [23] have shown that there exist four basic waves propagating with distinct phase speeds in an infinite micropolar elastic solid. They are as follows:

1. A longitudinal displacement wave traveling with phase speed V_1 given by

$$V_1^2=\frac{\lambda+2\mu+K}{\rho}.$$

2. A longitudinal microrotational wave propagating with phase speed V_2 given as

$$V_2^2=\frac{\alpha+\beta+\gamma}{\rho J(1-\Omega)},$$

where $\Omega=2\omega_0^2/\omega^2, \omega_0^2=K/\rho J, \omega=kV$ is the circular frequency, k is the wavenumber and V is the phase speed of the wave. The longitudinal microrotational wave propagates with a speed V_2 with its microrotation vector in the direction of propagation.

3. Two sets of coupled transverse waves propagating with phase speeds $V_{3,4}$ given by

$$V_{3,4}^2=\frac{1}{2(1-\Omega)}\left\{\Gamma\pm\sqrt{\Gamma^2-4c_4^2(1-\Omega)(c_2^2+c_3^2)}\right\},$$

where the '+' and '−' signs correspond to V_3^2 and V_4^2, respectively, $c_4^2=\gamma/\rho J, c_2^2=\mu/\rho$, $c_3^2=K/\rho, \Gamma=c_4^2+c_2^2(1-\Omega)+c_3^2(1-\Omega/2)$ and Ω is defined earlier. Each set consists of a transverse displacement wave coupled with a transverse microrotational wave.

Non-centrosymmetric, isotropic micropolar solids can be described by the constitutive equations [11]:

$$\tau'_{ij}=\lambda' u'_{k,k}\delta_{ij}+\mu'(u'_{i,j}+u'_{j,i})+C_3\Phi'_{j,i}, \tag{6}$$

$$m'_{ij}=\alpha'\Phi'_{k,k}\delta_{ij}+\beta'\Phi'_{i,j}+\gamma'\Phi'_{j,i}+C_3u'_{j,i}-C_3e_{ijk}\Phi'_k, \tag{7}$$

where u'_j and Φ'_j are, respectively, the displacement and the microrotation vectors in an elastic chiral medium; τ'_{ij} is the force stress tensor, m'_{ij} is the couple stress tensor; $\lambda', \mu', \alpha', \beta'$ and γ' are the corresponding elastic parameters in the chiral medium and C_3 is the hemitropic constant.

The elastodynamic equations of an elastic chiral solid with vanished body force and body couple densities, are governed by (Ref. [12])

$$(\lambda'+\mu')\nabla\nabla\cdot\mathbf{u}'+\mu'\nabla^2\mathbf{u}'+C_3\nabla^2\mathbf{\Phi}'=\rho'\ddot{\mathbf{u}}', \tag{8}$$

$$(\alpha'+\beta')\nabla\nabla\cdot\mathbf{\Phi}'+\gamma'\nabla^2\mathbf{\Phi}'+2C_3\nabla\times\mathbf{\Phi}'+C_3\nabla^2\mathbf{u}'=\rho' J'\ddot{\mathbf{\Phi}}', \tag{9}$$

where ρ' and $\rho' J'$ are, respectively, the mass density and the moment of inertia per unit volume.

Decomposing the vectors $\mathbf{u}'$ and $\mathbf{\Phi}'$ by using the scalar potentials q' and ξ'; the vector potentials $\mathbf{U}'$ and $\mathbf{\Pi}'$, respectively, as we decomposed the vectors $\mathbf{u}$ and $\mathbf{\Phi}$ in (5) and inserting them into Eqs. (8)–(9), one can obtain the following equations (see Ref. [22]) after substituting the expression of plane harmonic wave

$$V'^4-[c'^2_1+c'^2_4+c'^2_5]V'^2+[c'^2_1(c'^2_4+c'^2_5)-c'^2_6c'^2_7]=0, \tag{10}$$

$$[(V'^2-c'^2_4)(V'^2-c'^2_2)-c'^2_6c'^2_7]^2k'^2-[2c'^2_7(c'^2_2-V'^2)]^2=0. \tag{11}$$

where k' is the wavenumber, $c'^2_1 = (\lambda' + 2\mu')/\rho', c'^2_2 = \mu'/\rho', c'^2_4 = \gamma'/\rho' J', c'^2_5 = (\alpha' + \beta')/\rho' J', c'^2_6 = C_3/\rho'$ and $c'^2_7 = c'^2_6/J' = C_3/\rho' J'$. Lakhtakia et al. [18] have shown that there exist 6 sets of basic waves traveling with different phase speeds in an infinite effective chiral medium. They are as follows:

1. Two sets of non-dispersive coupled longitudinal waves (each set consisting of a longitudinal displacement wave and a longitudinal microrotational wave) traveling with phase speeds V'_1 and V'_2. The phase speeds of these coupled longitudinal waves can be obtained from the Eq. (10) and the expressions of square of these phase speeds are given by

$$V'^2_{1,2} = \Gamma' \pm \sqrt{\Gamma'^2 - \{c'^2_1(c'^2_4 + c'^2_5) - c'^2_6 c'^2_7\}}, \quad \Gamma' = (c'^2_1 + c'^2_4 + c'^2_5)/2. \tag{12}$$

2. Four sets of dispersive-coupled transverse waves (each set consisting of a transverse displacement wave and a transverse microrotational wave) traveling with phase speeds V'_i $(i = 3, 4, 5, 6)$, where V'^2_i are the roots of Eq. (11). Out of these 4 distinct sets of coupled transverse waves, the 2 sets are coupled right circularly polarized (RCP) waves and the remaining two sets are the coupled left circularly polarized (LCP) waves.

Now, we consider a micropolar elastic solid in the upper half-space designated by the region R_1 $[z<0]$ and an elastic chiral solid in the lower half-space designated by the region R_2 $[z>0]$. We consider a train of time harmonic plane longitudinal displacement wave, i.e., $\propto \exp(\iota\omega t)$, propagating through the micropolar elastic solid half-space and striking at the interface $z = 0$ with making an angle θ_1 with the z-axis. To satisfy the boundary conditions at the interface, we take the following reflected and transmitted waves into consideration:

Reflected waves: (1) A longitudinal displacement wave traveling with speed V_1 and making an angle θ_2 with the normal. (2) Two sets of coupled transverse waves propagating with speeds $V_{3,4}$ and making angles $\theta_{3,4}$, respectively, with the normal.

Transmitted waves: (1) Two sets of coupled longitudinal waves traveling with speeds $V'_{1,2}$ and making angles $\theta'_{1,2}$, respectively, with the normal. (2) Four sets of coupled transverse waves propagating with phase speeds V'_i and making angles θ'_i $(i = 3, 4, 5, 6)$, respectively, with the normal.

The complete geometry of the problem is shown in Fig. 1. We take the following potentials in the region $R_1[z<0]$:

$$q = A_1 \exp\{\iota k_1(\sin\theta_1 x + \cos\theta_1 z) - \iota\omega_1 t\} + A_2 \exp\{\iota k_1(\sin\theta_2 x - \cos\theta_2 z) - \iota\omega_1 t\}, \tag{13}$$

$$\mathbf{U} = \sum_{p=3}^{4} A_{py}\hat{\mathbf{e}}_y \exp\{\iota k_p(\sin\theta_p x - \cos\theta_p z) - \iota\omega_p t\}, \tag{14}$$

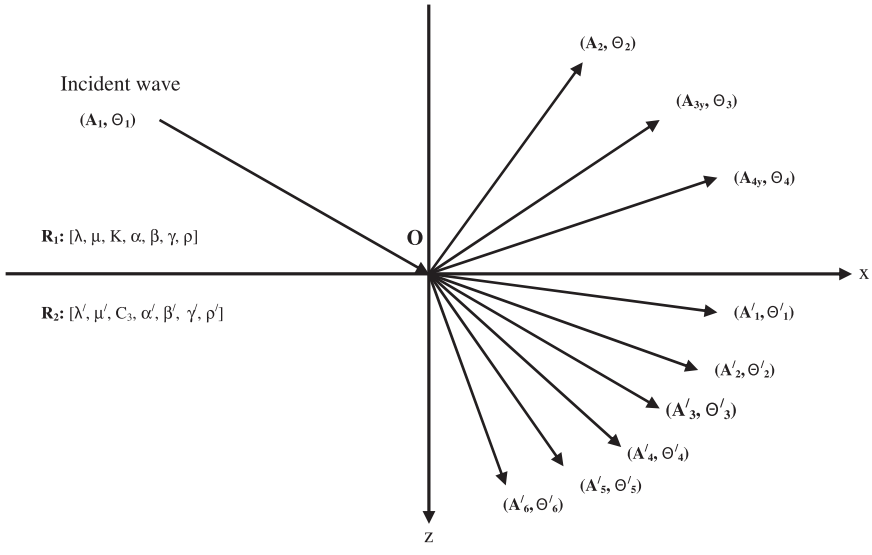

Fig. 1. The geometry of the problem.

$$\mathbf{\Pi} = \sum_{p=3}^{4} (B_{px}\hat{\mathbf{e}}_x + B_{pz}\hat{\mathbf{e}}_z) \exp\{\iota k_p(\sin\theta_p x - \cos\theta_p z) - \iota\omega_p t\} \tag{15}$$

and the potentials in the region R_2 $[z>0]$,

$$q' = \sum_{p=1}^{2} A'_p \exp\{\iota k'_p(\sin\theta'_p x + \cos\theta'_p z) - \iota\omega'_p t\}, \tag{16}$$

$$\mathbf{U}' = \sum_{p=3}^{6} A'_p(\triangle_p^1\hat{\mathbf{e}}_x + \triangle_p^2\hat{\mathbf{e}}_y + \triangle_p^3\hat{\mathbf{e}}_z) \exp\{\iota k'_p(\sin\theta'_p x + \cos\theta'_p z) - \iota\omega'_p t\}, \tag{17}$$

$$\xi' = \sum_{p=1}^{2} D_p A'_p \exp\{\iota k'_p(\sin\theta'_p x + \cos\theta'_p z) - \iota\omega'_p t\}, \tag{18}$$

$$\mathbf{\Pi}' = \sum_{p=3}^{6} D_p A'_p(\triangle_p^1\hat{\mathbf{e}}_x + \triangle_p^2\hat{\mathbf{e}}_y + \triangle_p^3\hat{\mathbf{e}}_z) \exp\{\iota k'_p(\sin\theta'_p x + \cos\theta'_p z) - \iota\omega'_p t\}, \tag{19}$$

where $\omega_l = k_l V_l$ $(l = 1, 3, 4)$ and $\omega'_r = k'_r V'_r$ $(r = 1, 2, \ldots, 6)$ have been defined earlier; $\hat{\mathbf{e}}_x$, $\hat{\mathbf{e}}_y$ and $\hat{\mathbf{e}}_z$ are the Cartesian unit vectors; A_1 and A_2 denote the amplitudes of the incident and the reflected longitudinal displacement waves, respectively; $\mathbf{A}_p$ and $\mathbf{B}_p$ $(p = 3, 4)$ are respectively, the amplitudes of the reflected transverse displacement and the transverse microrotation waves, and A'_r $(r = 1, 2, \ldots, 6)$ are the amplitudes of the respective transmitted waves traveling with phase speeds V'_r. The coefficients $\mathbf{A}_p$ and $\mathbf{B}_p$ $(p = 3, 4)$ are related to each other through the relation given by (Ref. [23])

$$\mathbf{B}_p = \frac{\iota\omega_0^2 A_{py}}{k_p(c_4^2 + 2\omega_0^2 k_p^{-2} - V_p^2)}(\cos\theta_p\hat{\mathbf{e}}_x + \sin\theta_p\hat{\mathbf{e}}_z). \tag{20}$$

The expressions of D_p are given by (Ref. [29])

$$D_p = \begin{cases} \dfrac{\rho'\omega'^2 - k'^2_p(\lambda' + 2\mu')}{k'^2_p C_3}, & p = 1, 2, \\ \dfrac{\rho'\omega'^2 - k'^2_p\mu'}{k'^2_p C_3}, & p = 3, 4, 5, 6. \end{cases} \tag{21}$$

When a RCP or LCP plane wave propagates in the xz-plane, the presentation of $\triangle_p^1$, $\triangle_p^2$ and $\triangle_p^3$ can be specified as

$$\triangle_p^1 : \triangle_p^2 : \triangle_p^3 = \pm\iota\cos\theta'_p : 1 : \mp\iota\sin\theta'_p,$$

where the upper signs '+' in $\triangle_p^1$ and '−' in $\triangle_p^3$ refer to the RCP plane waves, and the lower signs '−' in $\triangle_p^1$ and '+' in $\triangle_p^3$ refer to the LCP plane waves.

We have 9 unknown in (13)–(19); so we need 9 linearly independent boundary conditions at the plane interface $z = 0$. Classical elasticity theory provides us the following 6 conditions: At $z = 0$ (see Ref. [26])

$$\mathbf{u}'^{(\mathrm{tr})} = \mathbf{u}^{(\mathrm{ref})} + \mathbf{u}^{(\mathrm{inc})}, \tag{22}$$

$$\hat{\mathbf{e}}_z \cdot \boldsymbol{\tau}'^{(\mathrm{tr})} = \hat{\mathbf{e}}_z \cdot (\boldsymbol{\tau}^{(\mathrm{ref})} + \boldsymbol{\tau}^{(\mathrm{inc})}). \tag{23}$$

In addition, the following three boundary conditions on microrotation field are required at $z = 0$:

$$\mathbf{\Phi}'^{(\mathrm{tr})} = \mathbf{\Phi}^{(\mathrm{ref})}. \tag{24}$$

Eqs. (22)–(24) constitute a set (say Set-I) of boundary conditions and are suffice to solve the boundary value problem. However, there is another set (say Set-II) of boundary conditions possible as well at the interface

which comprise of the continuity of the normal component of the couple stress, i.e., at $z = 0$

$$\hat{\mathbf{e}}_z \cdot \mathbf{m}'^{(\mathrm{tr})} = \hat{\mathbf{e}}_z \cdot (\mathbf{m}^{(\mathrm{ref})} + \mathbf{m}^{(\mathrm{inc})}), \tag{25}$$

together with the conditions mentioned in Eqs. (22) and (23).

Since it is well-known that the difference between the micropolar elasticity and that of the classical elasticity is the introduction of microrotation ($\mathbf{\Phi}$) and couple stress ($\mathbf{m}$). Thus, in a micropolar-chiral problem, both the microrotation and couple stress are continuous at the interface. It can be seen that whichever set of boundary conditions is used, a system of 9 equations will be obtained (see Refs. [22,27]). In the present problem, we have obtained the solution for the unknown using both the possible sets (Set-I and Set-II) of boundary conditions given by Eqs. (22)–(24) and Eqs. (22), (23) and (25), respectively.

The potentials given in (13)–(19) will satisfy the Set-I of boundary conditions if $k_l \sin\theta_l = k_1 \sin\theta_2 = k'_r \sin\theta'_r$, $\omega_l = \omega'_r = \omega$ $(l = 1, 3, 4; r = 1, 2, \ldots, 6)$ and

$$\sin\theta_1 k_1 A_1 + \sin\theta_2 k_1 A_2 + \sum_{p=3}^{4} \cos\theta_p k_p A_{py} = \sum_{p=1}^{2} \sin\theta'_p k'_p A'_p - \sum_{p=3}^{6} \cos\theta'_p k'_p A'_p, \tag{26}$$

$$\sum_{p=3}^{4} k'_p A'_p - \sum_{p=5}^{6} k'_p A'_p = 0, \tag{27}$$

$$\cos\theta_1 k_1 A_1 - \cos\theta_2 k_1 A_2 + \sum_{p=3}^{4} \sin\theta_p k_p A_{py} = \sum_{p=1}^{2} \cos\theta'_p k'_p A'_p + \sum_{p=3}^{6} \sin\theta'_p k'_p A'_p, \tag{28}$$

$$\begin{aligned}&(2\mu + K)\sin\theta_1 \cos\theta_1 k_1^2 A_1 - (2\mu + K)\sin\theta_2 \cos\theta_2 k_1^2 A_2 \\ &\quad - \sum_{p=3}^{4} \left(\mu \cos 2\theta_p + K\cos^2\theta_p - \frac{K\omega_0^2}{k_p^2(c_4^2 + 2\omega_0^2 k_p^{-2} - V_p^2)} \right) k_p^2 A_{py} \\ &\quad = \sum_{p=1}^{2} (2\mu' + C_3 D_p)\sin\theta'_p \cos\theta'_p k'^2_p A'_p - \sum_{p=3}^{6} (\mu' \cos 2\theta'_p + C_3 \cos^2\theta'_p D_p) k'^2_p A'_p,\end{aligned} \tag{29}$$

$$\sum_{p=3}^{4} (\mu' + C_3 D_p)\cos\theta'_p k'^2_p A'_p - \sum_{p=5}^{6} (\mu' + C_3 D_p)\cos\theta'_p k'^2_p A'_p = 0, \tag{30}$$

$$\begin{aligned}&[\lambda + (2\mu + K)\cos^2\theta_1] k_1^2 A_1 + [\lambda + (2\mu + K)\cos^2\theta_2] k_1^2 A_2 - (2\mu + K) \sum_{p=3}^{4} \sin\theta_p \cos\theta_p k_p^2 A_{py} \\ &= \sum_{p=1}^{2} [\lambda' + (2\mu' + C_3 D_p)\cos^2\theta'_p] k'^2_p A'_p + \sum_{p=3}^{6} (2\mu' + C_3 D_p)\sin\theta'_p \cos\theta'_p k'^2_p A'_p,\end{aligned} \tag{31}$$

$$\sum_{p=1}^{2} \sin\theta'_p D_p k'_p A'_p - \sum_{p=3}^{6} \cos\theta'_p D_p k'_p A'_p = 0, \tag{32}$$

$$\sum_{p=3}^{4} \frac{\omega_0^2 A_{py}}{c_4^2 + 2\omega_0^2 k_p^{-2} - V_p^2} = \sum_{p=3}^{4} D_p k'_p A'_p - \sum_{p=5}^{6} D_p k'_p A'_p, \tag{33}$$

$$\sum_{p=1}^{2} \cos\theta'_p D_p k'_p A'_p + \sum_{p=3}^{6} \sin\theta'_p D_p k'_p A'_p = 0. \tag{34}$$

Eqs. (26)–(34) obtained by utilizing Set-I of boundary conditions can be written in matrix form as

$$MX = N, \tag{35}$$

where $M = [a_{ij}]$ is a 9×9 matrix, N is a 9×1 matrix, $X = [Z_1, Z_2, Z_3, Z'_1, Z'_2, Z'_3, Z'_4, Z'_5, Z'_6]^t$, $Z_1 = A_2/A_1, Z_2 = A_{3y}/A_1, Z_3 = A_{4y}/A_1$ are the reflection coefficients and $Z'_r = A'_r/A_1$ $(r = 1, 2, \ldots, 6)$ are the transmission coefficients. The non-vanishing elements of the coefficient matrix M together with the elements of the column matrix N are given in Appendix A. A non-homogeneous system of equations similar to Eqs. (26)–(34) can be obtained by utilizing Set-II of boundary equations and they can be written in the matrix form similar to Eq. (35). The non-zero elements of the matrix M obtained using Set-II which distinguish from the elements of Set-I are given in Appendix B. Eq. (35) will enable us to determine the amplitude ratios of various reflected and transmitted waves.

3. Limiting cases

1. If we assume that the half-space R_1 is free from micropolarity then we will be left with the relevant problem at an achiral–chiral interface. In this limiting case, we see that $\mathbf{B}_p = \mathbf{0}$. Also, the phase speed V_4 would be zero (see Ref. [20]). Thus, the wave propagating with phase speed V_4 will not appear in the medium R_1. Hence, after making the required substitutions, the Eqs. (26)–(34) will reduce to the equations that are analogous to the equations obtained by Lakhtakia et al. [24].

2. If micropolar effect is removed from the half-space R_1 and the chirality and microrotation effects are removed from the half-space R_2, then the problem will reduce to an elastic–elastic solid interface. In this case, the roots of Eq. (10) are $V'^2_1 = (\lambda' + 2\mu')/\rho'$ and $V'^2_2 = 0$, while Eq. (11) have two non-zero equal roots, one of them corresponds to a LCP wave and the other corresponds to a RCP wave, propagating with the same phase speed, i.e., $\sqrt{\mu'/\rho'}$. Here, the boundary conditions will be corresponding to displacement and normal component of force stress only. With these considerations, the matrix equation (35) obtained by utilizing both the possible sets of boundary conditions exactly match with the corresponding equations obtained by Miklowitz [28] for the relevant problem.

4. Numerical results and discussion

We have computed the square of phase speeds of all the coupled transverse plane waves existing in an elastic chiral solid medium and the modulus of amplitude ratios of various reflected and transmitted waves using two possible sets of boundary conditions, for a model having the following values of the relevant parameters:

For a micropolar elastic solid half-space (see Ref. [29])

$$\lambda = 75900 \times 10^6\,\mathrm{N/m^2},\ \ \mu = 13500 \times 10^6\,\mathrm{N/m^2},\ \ K = 149 \times 10^6\,\mathrm{N/m^2},\ \ \rho = 2200\,\mathrm{kg/m^3},$$

$$J = 0.00000196\,\mathrm{m^2},\ \ \alpha = 0.01 \times 10^6\,\mathrm{N},\ \ \beta = 0.015 \times 10^6\,\mathrm{N},\ \ \gamma = 0.0268 \times 10^6\,\mathrm{N}\ \text{ and }\ \omega/\omega_0 = 10.$$

For an elastic chiral solid half-space (see Ref. [8])

$$\lambda' = 500 \times 10^6\,\mathrm{N/m^2},\ \ \mu' = 300 \times 10^6\,\mathrm{N/m^2},\ \ J' = 0.01\,\mathrm{m^2},\ \ \rho' = 1200\,\mathrm{kg/m^3},$$

$$\alpha' = 2.0 \times 10^6\,\mathrm{N},\ \ \beta' = 4.0 \times 10^6\,\mathrm{N},\ \ \gamma' = 5.0 \times 10^6\,\mathrm{N}\ \text{ and }\ C_3 = 20.0 \times 10^6\,\mathrm{N/m}.$$

Figs. 2 and 3 depict the variations of square of phase speeds V'^2_i $(i = 3, 4, 5, 6)$ of the coupled transverse waves existing in the chiral elastic medium with the frequency ratio (ω/ω_0) lying in the range $0 \leqslant \omega/\omega_0 \leqslant 5000$. It can be seen that in the initial range of frequency ratio, V'^2_3 and V'^2_4 increase, while V'^2_5 and V'^2_6 decrease with increase in the frequency ratio. However, at higher values of the frequency ratio, the square of speeds of each set of these coupled transverse waves approach toward certain constant values. The variations (increase or decrease) of square of these phase speeds in the initial frequency range are very small from their constant values at higher frequency.

In Fig. 4, we have plotted the modulus values of the reflection coefficients obtained by utilizing Set-I of boundary conditions, as a function of the angle of incidence. The reflection coefficient Z_1 begins with the value

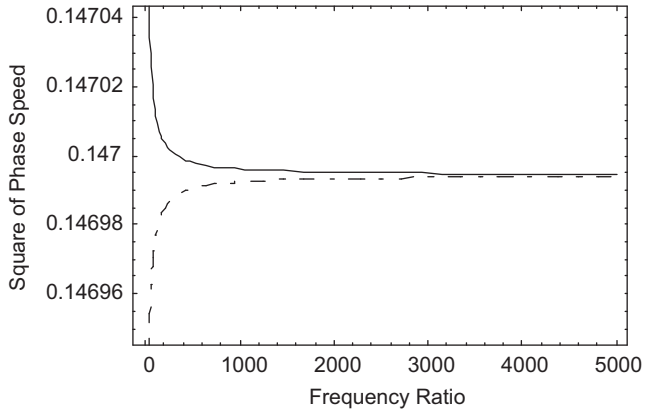

Fig. 2. The variations of $V_3'^2$ (dashed curve) and $V_5'^2$ (solid curve) with frequency ratio (ω/ω_0).

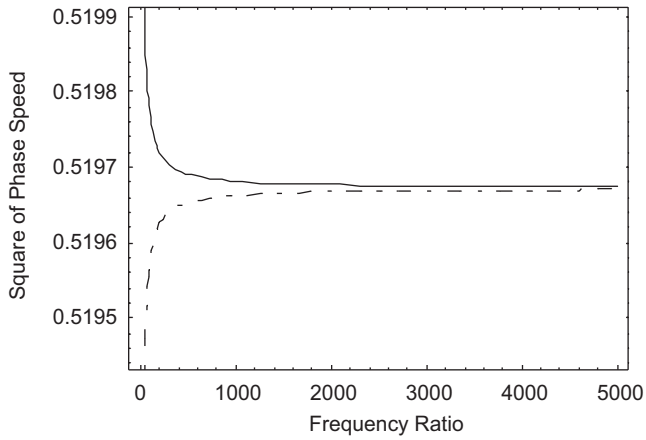

Fig. 3. The variations of $V_4'^2$ (dashed curve) and $V_6'^2$ (solid curve) with frequency ratio (ω/ω_0).

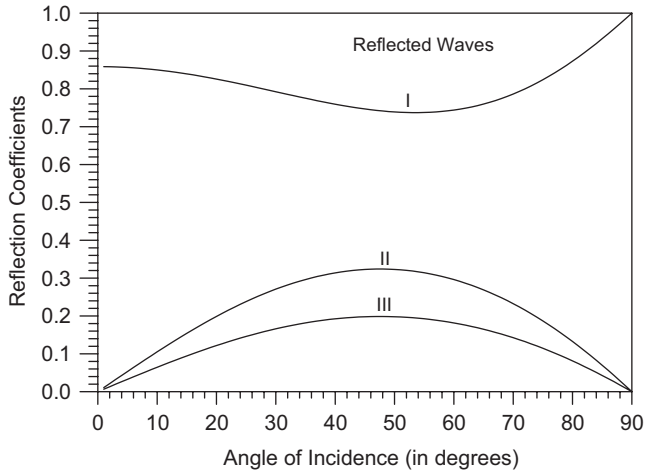

Fig. 4. The variations of modulus of reflection coefficients with angle of incidence of longitudinal wave propagating with phase speed V_1 (Curve I: Z_1, Curve II: $Z_2 \times 10$, Curve III: Z_3).

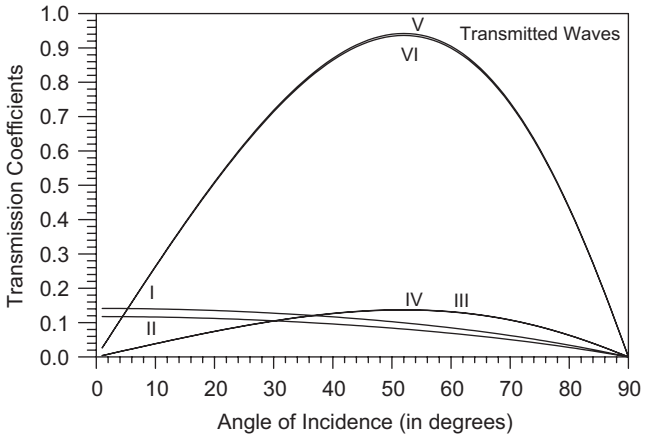

Fig. 5. The variations of modulus of transmission coefficients with angle of incidence of longitudinal wave propagating with phase speed V_1 (Curve I: Z'_1, Curve II: Z'_2, Curve III: $Z'_3 \times 10$, Curve IV: $Z'_4 \times 10$, Curve V: $Z'_5 \times 10^2$, Curve VI: $Z'_6 \times 10^2$).

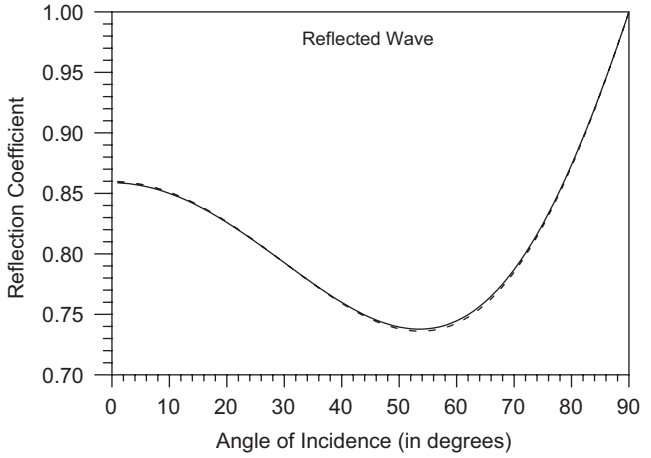

Fig. 6. The variations of modulus of reflection coefficient Z_1 corresponding to the reflected wave propagating with phase speed V_1 with angle of incidence, using Set-I (solid curve) and Set-II (dashed curve).

0.8587 near the normal incidence, then it decreases with increase in the angle of incidence θ_1 lying in the range $1^\circ \leqslant \theta_1 \leqslant 54^\circ$, and attains the value 0.7371 at $\theta_1 = 54^\circ$, thereafter, the reflection coefficient Z_1 increases and approaches to its maximum value, i.e., unity, at the grazing incidence. The reflection coefficients Z_2 and Z_3 increase with increase in the angle of incidence till $\theta_1 = 48^\circ$, then their values decrease and approach to zero as θ_1 approaches grazing incidence. We have plotted the reflection coefficient Z_2 after magnifying its original value by the factor 10.

In Fig. 5, we have shown the variations of modulus values of the transmission coefficients with the angle of incidence. The transmission coefficients Z'_1 and Z'_2 begin with their maximum values, i.e., 0.1413 and 0.1176, respectively, near the normal incidence and then they decrease with increase in the angle of incidence. The transmission coefficients Z'_3 and Z'_4 begin with the value zero near the normal incidence, then both the transmission coefficients increase slowly with increase in the angle of incidence till $\theta_1 = 52^\circ$. Beyond $\theta_1 = 52^\circ$, these transmission coefficients decrease rapidly and approach to zero as θ_1 approaches 90°. The pattern of transmission coefficient Z'_5 is almost similar to that of Z'_6 with respect to the angle of incidence. Both these transmission coefficients begin with the value zero near the normal incidence, then both increase sharply with increase in the angle of incidence and attain their respective maximum values at $\theta_1 = 52^\circ$ and decrease afterwards. We have plotted the transmission coefficients Z'_3, Z'_4, Z'_5 and Z'_6 after magnifying their original values with the factors $10, 10, 10^2$ and 10^2, respectively.

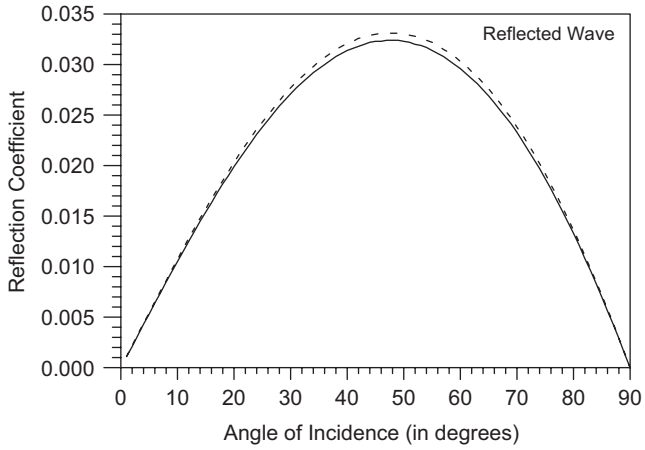

Fig. 7. The variations of modulus of reflection coefficient Z_2 corresponding to the reflected wave propagating with phase speed V_3 with angle of incidence, using Set-I (solid curve) and Set-II (dashed curve).

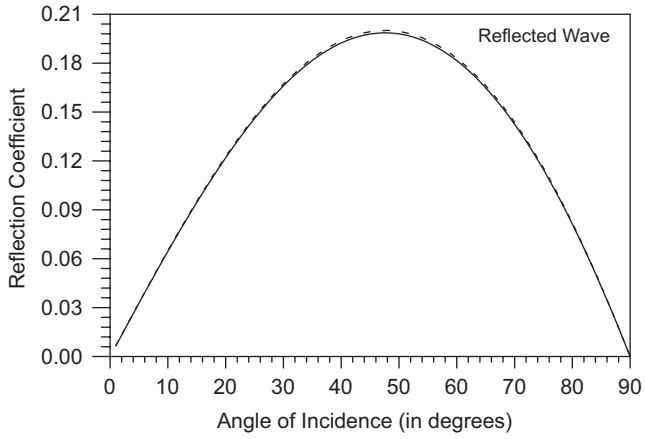

Fig. 8. The variations of modulus of reflection coefficient Z_3 corresponding to the reflected wave propagating with phase speed V_4 with angle of incidence, using Set-I (solid curve) and Set-II (dashed curve).

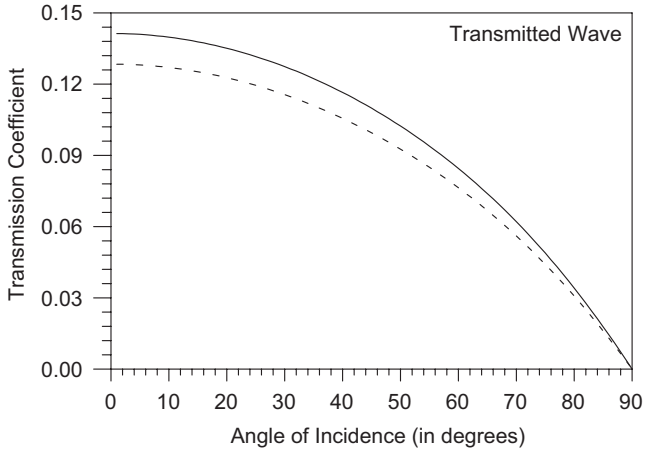

Fig. 9. The variations of modulus of transmission coefficient Z_1' corresponding to the transmitted wave propagating with phase speed V_1' with angle of incidence, using Set-I (solid curve) and Set-II (dashed curve).

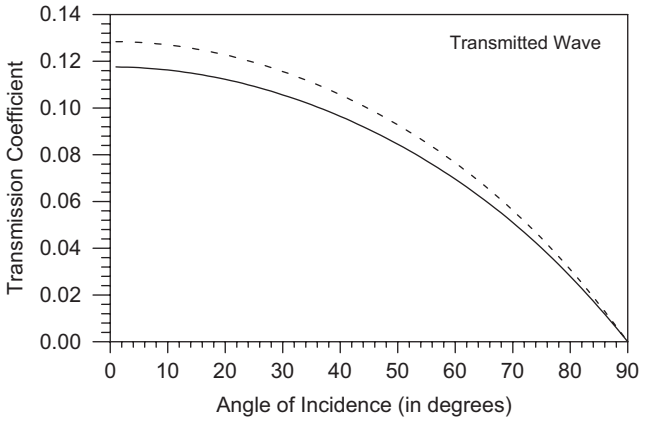

Fig. 10. The variations of modulus of transmission coefficient Z_2' corresponding to the transmitted wave propagating with phase speed V_2' with angle of incidence, using Set-I (solid curve) and Set-II (dashed curve).

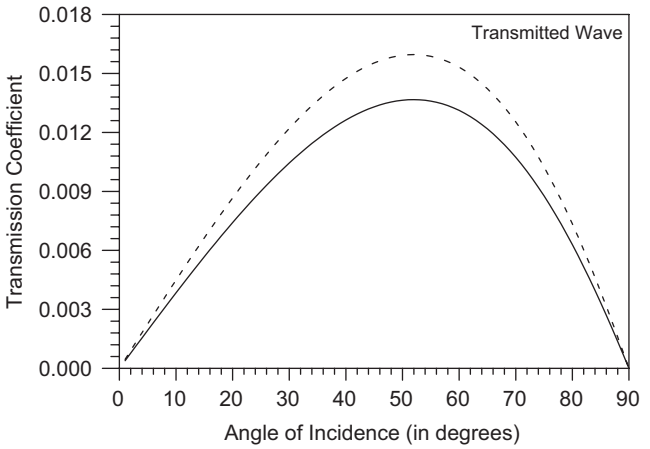

Fig. 11. The variations of modulus of transmission coefficient Z_3' corresponding to the transmitted wave propagating with phase speed V_3' with angle of incidence, using Set-I (solid curve) and Set-II (dashed curve).

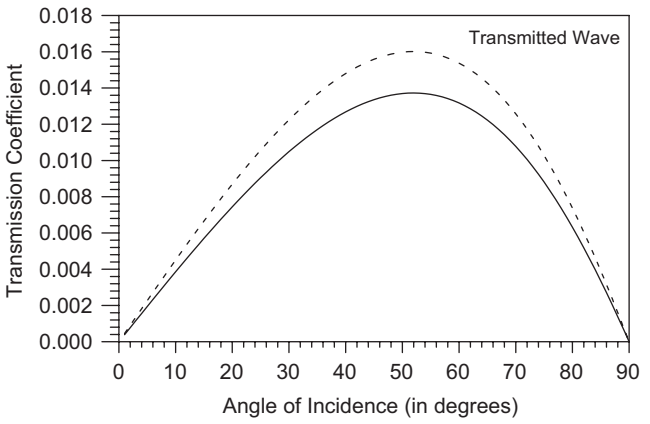

Fig. 12. The variations of modulus of transmission coefficient Z_4' corresponding to the transmitted wave propagating with phase speed V_4' with angle of incidence, using Set-I (solid curve) and Set-II (dashed curve).

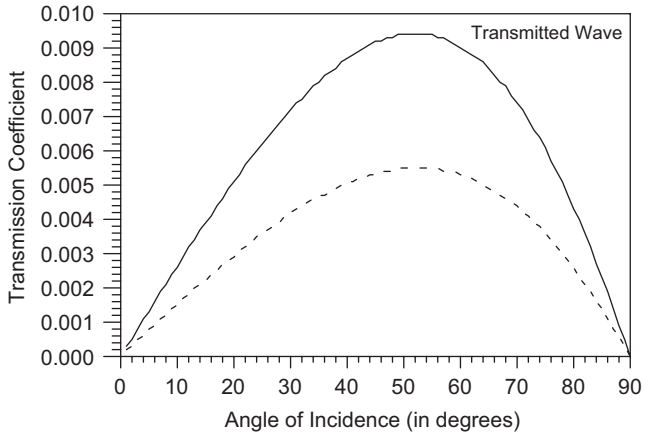

Fig. 13. The variations of modulus of transmission coefficient Z_5' corresponding to the transmitted wave propagating with phase speed V_5' with angle of incidence, using Set-I (solid curve) and Set-II (dashed curve).

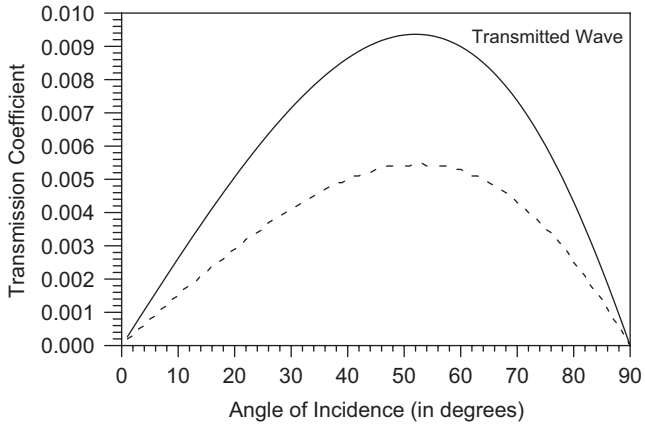

Fig. 14. The variations of modulus of transmission coefficient Z_6' corresponding to the transmitted wave propagating with phase speed V_6' with angle of incidence, using Set-I (solid curve) and Set-II (dashed curve).

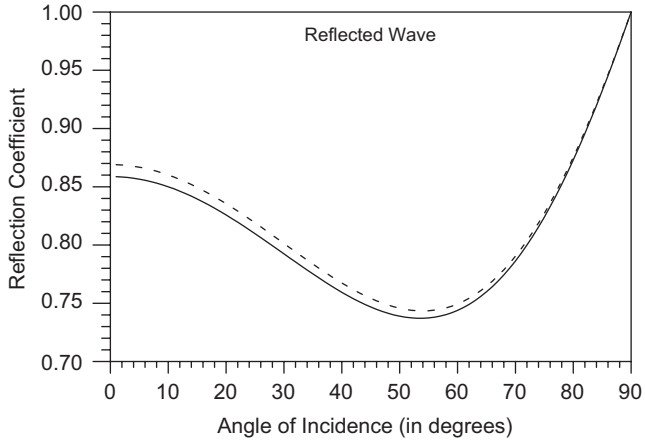

Fig. 15. The effect of hemitropic parameter (C_3) on the modulus of reflection coefficient Z_1 with angle of incidence of longitudinal wave propagating with phase speed V_1 (Solid curve at $C_3 = 20 \times 10^6$ N/m, dashed curve at $C_3 = 80 \times 10^6$ N/m).

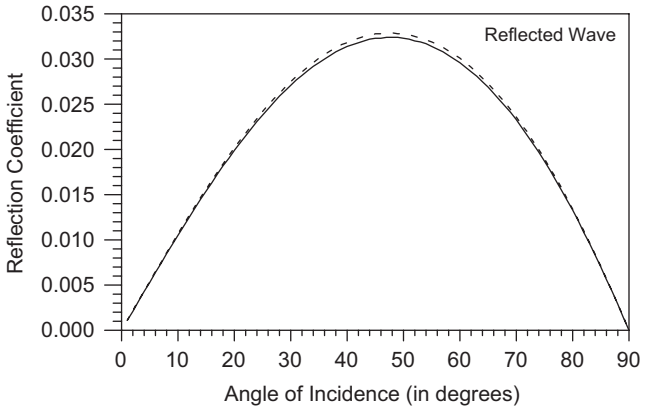

Fig. 16. The effect of hemitropic parameter (C_3) on the modulus of reflection coefficient Z_2 with angle of incidence of longitudinal wave propagating with phase speed V_1 (Solid curve Z_2 at $C_3 = 20 \times 10^6$ N/m, dashed curve Z_2 at $C_3 = 80 \times 10^6$ N/m).

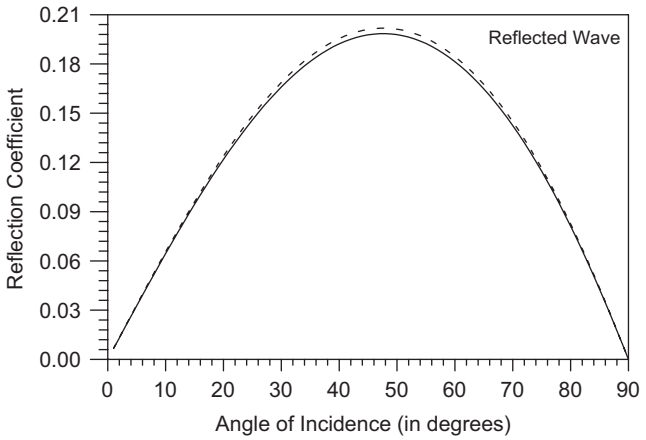

Fig. 17. The effect of hemitropic parameter (C_3) on the modulus of reflection coefficient Z_3 with angle of incidence of longitudinal wave traveling with phase speed V_1 (Solid curve at $C_3 = 20 \times 10^6$ N/m, dashed curve at $C_3 = 80 \times 10^6$ N/m).

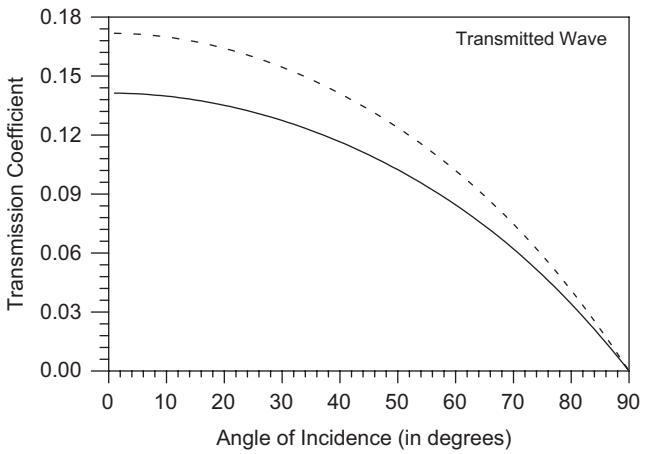

Fig. 18. The effect of hemitropic constant (C_3) on the modulus of transmission coefficient Z_1' corresponding to the wave propagating with phase speed V_1' when longitudinal wave is incident (Solid curve at $C_3 = 20 \times 10^6$ N/m, dashed curve at $C_3 = 80 \times 10^6$ N/m).

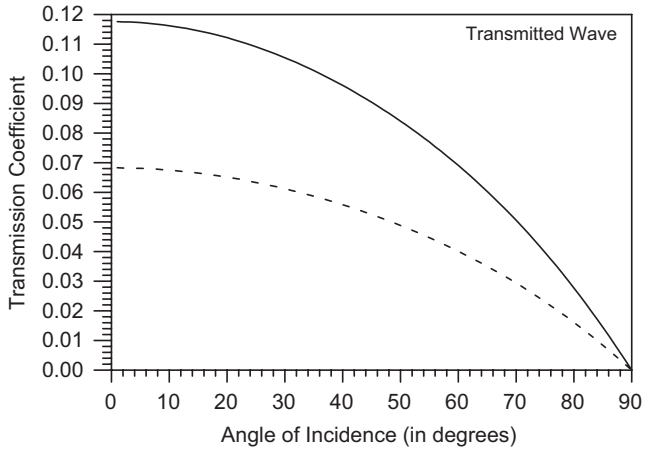

Fig. 19. The effect of hemitropic constant (C_3) on the modulus of transmission coefficient Z_2' corresponding to the wave propagating with phase speed V_2' when longitudinal wave is incident (Solid curve at $C_3 = 20 \times 10^6$ N/m, dashed curve at $C_3 = 80 \times 10^6$ N/m).

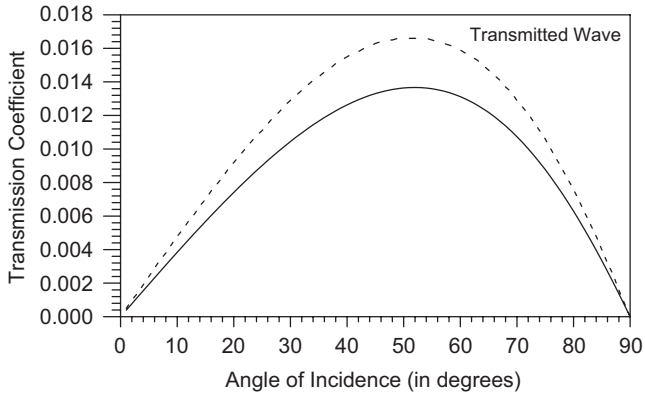

Fig. 20. The effect of hemitropic constant (C_3) on the modulus of transmission coefficient Z_3' corresponding to the wave propagating with phase speed V_3' when longitudinal wave is incident (Solid curve at $C_3 = 20 \times 10^6$ N/m, dashed curve at $C_3 = 80 \times 10^6$ N/m).

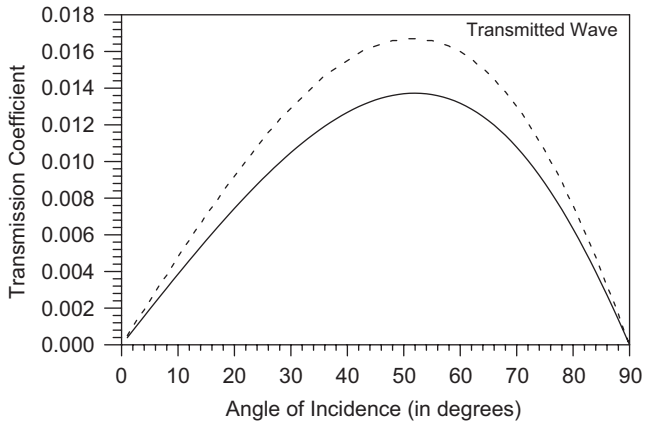

Fig. 21. The effect of hemitropic constant (C_3) on the modulus of transmission coefficient Z_4' corresponding to the wave propagating with phase speed V_4' when longitudinal wave is incident (Solid curve at $C_3 = 20 \times 10^6$ N/m, dashed curve at $C_3 = 80 \times 10^6$ N/m).

In Figs. 6–14, we have shown the comparison in the respective modulus values of reflection and transmission coefficients obtained by using the Set-I and II of boundary conditions, against the angle of incidence of longitudinal wave propagating with phase speed V_1.

In Fig. 6, it can be seen that at each angle of incidence, the value of reflection coefficient Z_1 obtained using Set-I and II attains almost equal value.

In Figs. 7, 8, 10–12 the modulus values of the amplitude ratios Z_2, Z_3, Z_2', Z_3' and Z_4' obtained using Set-II are bigger in comparison to their values obtained using Set-I, at each angle of incidence.

In Figs. 9, 13 and 14, the absolute values of the amplitude ratios Z_1', Z_5' and Z_6' obtained using Set-I are greater at each angle of incidence in comparison with those obtained by using Set-II.

Next, we have shown the variations of reflection and transmission coefficients obtained using Set-I of boundary conditions with the angle of incidence of longitudinal displacement wave propagating with phase speed V_1 at two different values of hemitropic constant namely, $C_3 = 20 \times 10^6$ N/m and 80×10^6 N/m. It is evident that the amplitude ratios depend on the angle of incidence as well as on the chirality parameter. The nature of this dependence on the angle of incidence and the chirality parameter is however, different for different reflected and transmitted waves.

In Fig. 15, we observed that at each angle of incidence lying in the range $1^\circ \leqslant \theta_1 \leqslant 80^\circ$, the value of reflection coefficient Z_1 corresponding to the wave propagating with phase speed V_1 increases with increase in the value

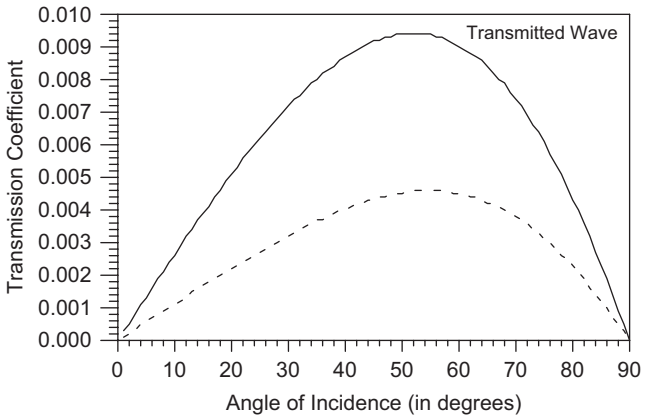

Fig. 22. The effect of hemitropic constant (C_3) on the modulus of transmission coefficient Z_5' corresponding to the wave propagating with phase speed V_5' when longitudinal wave is incident (Solid curve at $C_3 = 20 \times 10^6$ N/m, dashed curve at $C_3 = 80 \times 10^6$ N/m).

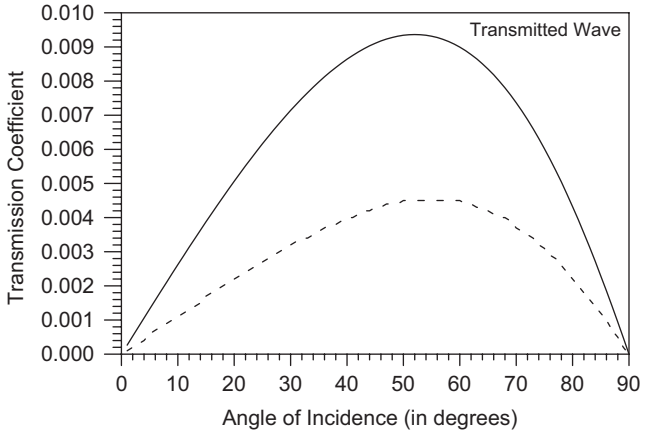

Fig. 23. The effect of hemitropic constant (C_3) on the modulus of transmission coefficient Z_6' corresponding to the wave propagating with phase speed V_6' when longitudinal wave is incident (Solid curve at $C_3 = 20 \times 10^6$ N/m, dashed curve at $C_3 = 80 \times 10^6$ N/m).

of C_3. Beyond $\theta_1 = 80^\circ$, the amplitude ratio Z_1 has almost equal values at the two different mentioned values of C_3.

In Figs. 16–18, 20 and 21, the modulus values of the amplitude ratios Z_2, Z_3, Z_1', Z_3' and Z_4' increase with increase in the value of C_3 at each angle of incidence.

In Figs. 19, 22 and 23, we have seen that at each angle of incidence, the modulus values of the amplitude ratios Z_2', Z_5' and Z_6' decrease with increase in the value of C_3.

It can be noticed from Figs. 15–23 that the amplitude ratios of various reflected and transmitted waves of an incident longitudinal wave propagating with phase speed V_1 are significantly influenced by the hemitropic constant (C_3).

5. Conclusions

In this paper, we have presented the reflection and transmission phenomena of an incident longitudinal plane wave propagating through the micropolar elastic solid half-space towards the plane interface between micropolar/chiral elastic solids. We conclude that:

1. At normal incidence, the reflection and transmission of only longitudinal waves take place and no coupled transverse wave is found to reflect or transmit.
2. At grazing incidence, no reflection or transmission phenomena take place and the same wave propagates along the interface.
3. Amplitude ratios of various reflected and transmitted waves depend upon the angle of incidence and the chirality parameter.
4. The variations in the chirality parameter (C_3) affect significantly various reflection and transmission coefficients.

Acknowledgments

Authors are thankful to Council of Scientific and Industrial Research, New Delhi for providing financial assistance through Grant No. 09/135(0493)/2005/EMR-I in the form of SRF awarded to AK and through Grant No. 25 (0134)/04/EMR-II sanctioned to SKT for completing this study. Authors are also thankful to the unknown reviewers for suggesting valuable improvements in the manuscript.

Appendix A

The non-zero coefficients of the matrix M of Eq. (35) obtained by utilizing Set-I are given as

$$a_{11} = \sin\theta_1, \quad a_{12} = \sqrt{1 - v_{31}^2 \sin^2\theta_1}/v_{31}, \quad a_{13} = \sqrt{1 - v_{41}^2 \sin^2\theta_1}/v_{41}, \quad a_{1t} = -\sin\theta_1,$$

$$a_{1p} = \sqrt{1 - V_{p1}'^2 \sin^2\theta_1}/V_{p1}', \quad a_{1s} = \sqrt{1 - V_{s1}'^2 \sin^2\theta_1}/V_{s1}', \quad a_{2p} = 1/V_{p1}', \quad a_{2s} = -1/V_{s1}',$$

$$a_{31} = \cos\theta_1, \quad a_{32} = a_{33} = -\sin\theta_1, \quad a_{3t} = \sqrt{1 - V_{t1}'^2 \sin^2\theta_1}/V_{t1}', \quad a_{3p} = a_{3s} = \sin\theta_1,$$

$$a_{44} = \sin\theta_1, \quad a_{45} = D_2 \sin\theta_1/D_1, \quad a_{4p} = -D_{p-3}\sqrt{1 - V_{p1}'^2 \sin^2\theta_1}/(D_1 V_{p1}'),$$

$$a_{4s} = -D_{s-3}\sqrt{1 - V_{s1}'^2 \sin^2\theta_1}/(D_1 V_{s1}'), \quad a_{52} = S_1 k_3/(D_1 v_{31}), \quad a_{53} = S_2 k_4/(D_1 v_{41}),$$

$$a_{5p} = -D_{p-3}/(D_1 V_{p1}'), \quad a_{5s} = D_{s-3}/(D_1 V_{s1}'), \quad a_{64} = \sqrt{1 - v_{11}'^2 \sin^2\theta_1}/v_{11}',$$

$$a_{65} = D_2\sqrt{1 - v_{21}'^2 \sin^2\theta_1}/(D_1 v_{21}'), \quad a_{6p} = D_{p-3} \sin\theta_1/D_1, \quad a_{6s} = D_{s-3} \sin\theta_1/D_1,$$

$$a_{71} = \sin\theta_1 \cos\theta_1, \quad a_{72} = (\mu + K - KS_1)/(B_1 v_{31}^2) - \sin^2\theta_1,$$

$$a_{73} = (\mu + K - KS_2)/(B_1 v_{41}^2) - \sin^2\theta_1, \quad a_{7t} = (2\mu' + C_3 D_{t-3}) \sin\theta_1 \sqrt{1 - V_{t1}'^2 \sin^2\theta_1}/(B_1 V_{t1}'),$$

$$a_{7p} = -[\mu'(1 - 2V_{p1}'^2 \sin^2\theta_1) + C_3 D_{p-3}(1 - V_{p1}'^2 \sin^2\theta_1)]/(B_1 V_{p1}'^2),$$

$$a_{7s} = -[\mu'(1 - 2V_{s1}'^2 \sin^2\theta_1) + C_3 D_{s-3}(1 - V_{s1}'^2 \sin^2\theta_1)]/(B_1 V_{s1}'^2),$$

$$a_{8p} = (\mu' + C_3 D_{p-3}) \sqrt{1 - V_{p1}'^2 \sin^2\theta_1}/(\mu V_{p1}'^2),$$

$$a_{8s} = -(\mu' + C_3 D_{s-3}) \sqrt{1 - V_{s1}'^2 \sin^2\theta_1}/(\mu V_{s1}'^2), \quad a_{91} = 1,$$

$$a_{92} = -B_1 \sin\theta_1 \sqrt{1 - v_{31}^2 \sin^2\theta_1}/(B_2 v_{31}), \quad a_{93} = -B_1 \sin\theta_1 \sqrt{1 - v_{41}^2 \sin^2\theta_1}/(B_2 v_{41}),$$

$$a_{9t} = -[\lambda' + (2\mu' + C_3 D_{t-3})(1 - V_{t1}'^2 \sin^2\theta_1)]/(B_2 V_{t1}'^2),$$

$$a_{9p} = -(2\mu' + C_3 D_{p-3}) \sin\theta_1 \sqrt{1 - V_{p1}'^2 \sin^2\theta_1}/(B_2 V_{p1}'),$$

$$a_{9s} = -(2\mu' + C_3 D_{s-3}) \sin\theta_1 \sqrt{1 - V_{s1}'^2 \sin^2\theta_1}/(B_2 V_{s1}'),$$

where $B_1 = 2\mu + K, B_2 = \lambda + B_1 \cos^2\theta_1, S_1 = \omega_0^2/(c_4^2 k_3^2 + 2\omega_0^2 - \omega^2)$,

$$S_2 = \omega_0^2/(c_4^2 k_4^2 + 2\omega_0^2 - \omega^2), \quad t = 4, 5; \quad p = 6, 7; \quad s = 8, 9; \quad v_{31} = \frac{V_3}{V_1}, v_{41} = \frac{V_4}{V_1},$$

$$v_{r1}' = \frac{V_r'}{V_1} (r = 1, 2, \ldots, 6), \quad V_{41}' = v_{11}', \quad V_{51}' = v_{21}', \quad V_{61}' = v_{31}', \quad V_{71}' = v_{41}', \quad V_{81}' = v_{51}',$$

$V_{91}' = v_{61}'$, and the column matrix $[N] = [-\sin\theta_1, 0, \cos\theta_1, 0, 0, 0, \sin\theta_1 \cos\theta_1, 0, -1]^t$.

Appendix B

The non-zero elements of the matrix M of Eq. (35) obtained by using Set-II of boundary conditions, that are different from the elements obtained using Set-I are given as follows:

$$a_{4t} = ((\beta' + \gamma')D_{t-3} + C_3) \sin\theta_1 \sqrt{1 - V_{t1}'^2 \sin^2\theta_1}/(V_{t1}' C_3),$$

$$a_{4p} = \left[((\beta' + \gamma')D_{p-3} + C_3) V_{p1}'^2 \sin^2\theta_1 - \left(\gamma' D_{p-3} + C_3 - \frac{C_3 D_{p-3}}{k_{p-3}'}\right)\right] \Big/ (V_{p1}'^2 C_3),$$

$$a_{4s} = \left[((\beta' + \gamma')D_{s-3} + C_3) V_{s1}'^2 \sin^2\theta_1 - \left(\gamma' D_{s-3} + C_3 + \frac{C_3 D_{s-3}}{k_{s-3}'}\right)\right] \Big/ (V_{s1}'^2 C_3),$$

$$a_{52} = \gamma S_1 k_1 \sqrt{1 - v_{31}^2 \sin^2\theta_1}/(v_{31}^3 C_3), \quad a_{53} = \gamma S_2 k_1 \sqrt{1 - v_{41}^2 \sin^2\theta_1}/(v_{41}^3 C_3),$$

$$a_{54} = D_1 \sin\theta_1/k_1, \quad a_{55} = D_2 \sin\theta_1/k_1, \quad a_{5p} = \left(\gamma' D_{p-3} + C_3 - \frac{C_3 D_{p-3}}{k_{p-3}'}\right) \sqrt{1 - V_{p1}'^2 \sin^2\theta_1}/(V_{p1}'^2 C_3),$$

$$a_{5s} = -\left(\gamma' D_{s-3} + C_3 + \frac{C_3 D_{s-3}}{k'_{s-3}}\right)\sqrt{1 - V'^2_{s1}\sin^2\theta_1}/(V'^2_{s1} C_3),$$

$$a_{6t} = [\alpha' D_{t-3} + ((\beta' + \gamma')D_{t-3} + C_3)(1 - V'^2_{t1}\sin^2\theta_1)]/(V'^2_{t1} C_3),$$

$$a_{6p} = ((\beta' + \gamma')D_{p-3} + C_3)\sin\theta_1\sqrt{1 - V'^2_{p1}\sin^2\theta_1}/(V'_{p1} C_3),$$

$$a_{6s} = ((\beta' + \gamma')D_{s-3} + C_3)\sin\theta_1\sqrt{1 - V'^2_{s1}\sin^2\theta_1}/(V'_{s1} C_3),$$

where $v_{31}, v_{41}, V'_{t1}, V'_{p1}, V'_{s1}, S_1, S_2$ and column matrix N same as defined in Appendix A.

References

[1] A.C. Smith, Waves in micropolar elastic solids, *International Journal of Engineering Science* 5 (1967) 741–746.
[2] R.S. Lakes, Dynamical study of couple stress effects in human compact bone, *ASME Journal of Biomechanical Engineering* 104 (1982) 6–11.
[3] Y. Weitsman, Initial stresses and skin effects in a hemitropic Cosserat continuum, *ASME Journal of Applied Mechanics* 34 (1967) 160–164.
[4] F. Arago, Institute Imperial de France, *Memoires de la Classe des Sciences Mathematiques et Physiques de* 1 (1811) 93.
[5] J.B. Biot, Institute Imperial de France, *Memoires de la Classe des Sciences Mathematiques et Physiques de* 1 (1812) 1.
[6] J.B. Biot, *Memories de l' Academie Royale des Sciences de l' Institut de France* 2 (1817) 41.
[7] A. Fresnel, *Oeuvres Completes*, Imperial Press, Paris, 1866.
[8] J.C. Bose, On the rotation plane of polarisation of electric waves by a twisted structure, *Proceedings of Royal Society London A* 63 (1898) 146–152.
[9] R. Ro, V.V. Varadan, V.K. Varadan, Electromagnetic activity and absorption in microwave chiral composites: H (Microwaves, Antennas and Propagation), *IEE Proceedings* 139 (1992) 441–448.
[10] H. Cory, I. Rosenhouse, *Electromagnetics* 17 (1997) 317.
[11] R.S. Lakes, R.L. Benedict, Noncentrosymmetry in micropolar elasticity, *International Journal of Engineering Science* 20 (1982) 1161–1167.
[12] W. Nowacki, *Theory of Asymmetric Elasticity*, Pergamon, Oxford, 1986.
[13] E.V. Kuvshinskii, E.L. Aero, Continuum theory of asymmetric elasticity, *Fizika Tverdogo Tela* 5 (1963) 2592 (in Russian).
[14] E.V. Kuvshinskii, E.L. Aero, Continuum theory of asymmetric elasticity equilibrium of anisotropic body, *Physics of Solids* 6 (1965) 2141–2148.
[15] E.L. Aero, E.V. Kuvshinskii, Continuum theory of asymmetric elasticity equilibrium of isotropic body, *Fizika Tverdogo Tela* 6 (1964) 2689 (in Russian).
[16] A.C. Eringen, Theory of micropolar elasticity, in: H. Leibowitz (Ed.), *Fracture*, Vol. I, Academic Press, New York, 1968.
[17] R. Ro, V.V. Varadan, V.K. Varadan, Experimental study of chiral composites, *Proceedings of SPIE—The International Society for Optical Engineering* 1558 (1991) 269–287.
[18] A. Lakhtakia, V.V. Varadan, V.K. Varadan, Elastic wave propagation in noncentrosymmetric, isotropic media: Dispersion and field equations, *Journal of Applied Physics* 63 (1988) 5246–5250; 64 (1988) 4795.
[19] S.K. Yang, S.Y. Hsia, Wave propagation in effective chiral composites (I) the characteristics of dispersion equations, *Proceedings of Eighth Asia-Pacific Conference NDT*, 1995, pp. 303–309.
[20] S.K. Tomar, M.L. Gogna, Reflection and refraction of a longitudinal microrotational wave at an interface between two micropolar elastic solids in welded contact, *International Journal of Engineering Science* 30 (1992) 1637–1646.
[21] S.K. Tomar, M.L. Gogna, Reflection and refraction of longitudinal wave at an interface between two micropolar elastic solids in welded contact, *Journal of the Acoustical Society of America* 97 (1995) 822–830; 102 (1997) 2452.
[22] M.J. Elphinstone, A. Lakhtakia, Plane-wave response of an elastic chiral solid slab sandwiched between achiral solid half-spaces, *Journal of the Acoustical Society of America* 95 (1994) 617–627.
[23] V.R. Parfitt, A.C. Eringen, Reflection of plane waves from the flat boundary of a micropolar elastic half-space, *Journal of the Acoustical Society of America* 45 (1969) 1258–1272.
[24] A. Lakhtakia, V.K. Varadan, V.V. Varadan, Reflection of elastic plane waves at a planar achiral-chiral interface, *Journal of the Acoustical Society of America* 87 (1990) 2314–2318.
[25] A.C. Eringen, Linear theory of micropolar elasticity, *Journal of Mathematics and Mechanics* 15 (1966) 909–923.
[26] J.D. Achenbach, *Wave Propagation in Elastic Solids*, North-Holland, Amsterdam, 1973.
[27] M.J. Elphinstone, A. Lakhtakia, Planewave response of an elastic chiral solid slab sandwiched between achiral fluid half-spaces, *Proceedings of the Indian National Science Academy A* 60 (1994) 593–605.
[28] J. Miklowitz, *The Theory of Elastic Waves and Waveguides*, North-Holland, New York, 1978.
[29] S.K. Tomar, M. Garg, Reflection and transmission of waves from a plane interface between two microstretch solid half spaces, *International Journal of Engineering Science* 43 (2005) 139–169; 44 (2006) 285–287.